Materials and Design 46 (2013) 776–783

Contents lists available at SciVerse ScienceDirect

Materials and Design

journal homepage: www.elsevier.com/locate/matdes

Technical Report

Investigation of electrochemical corrosion behavior in a 3.5 wt.% NaCl solution of boronized dual-phase steel

Yusuf Kayali [a,*], Bilal Anaturk [b]

[a] Afyon Kocatepe University, Technology Faculty, Department of Metallurgical and Materials Engineering, Afyon 03200, Turkey
[b] Afyon Kocatepe University, Institute of Natural and Applied Sciences, Department of Metal Education, Afyon 03200, Turkey

ARTICLE INFO

Article history:
Received 17 September 2012
Accepted 22 November 2012
Available online 29 November 2012

ABSTRACT

In this study, corrosion behaviors of boronized and non-boronized dual-phase steel were investigated with Tafel extrapolation and linear polarization methods in a 3.5 wt.% NaCl solution. Microstructure analyses show that the boride layer on the dual-phase steel surface had a flat and saw smooth morphology. It was detected by X-ray diffraction (XRD) analysis that the boride layer contained FeB and Fe_2B phases. The amount of martensite increases with an increase in the intercritical annealing temperature. Both the amount of martensite and the morphology of the phase constituents have an influence on the corrosion behavior of dual-phase steel. A higher corrosion tendency was observed with an increased amount of martensite. The corrosion resistance of boronized dual-phase steel is higher compared with that of dual-phase steel.

1. Introduction

Dual phase (DP) steel consists of hard martensite islands buried in a relatively soft and ductile matrix of ferrite [1–3]. In order to achieve these microstructures, it is sufficient to subject the steel to a heat treatment in the intercritical region [4]. This heat treatment consists of annealing between the critical temperatures of A1 and A3 and rapid cooling steps [5,6]. DP steels are characterized by an interesting combination of high strength, good ductility, continuous yielding, high initial work hardening rates, and a low yield stress to tensile strength ratio [7,8]. Besides, they have recently emerged as a potential engineering material system for automobile and other engineering applications [1,2]. However, the poor corrosion resistance of dual-phase steel as compared with stainless steel restricts the application of the former in the vehicle industry, especially in the outer panels of automobiles [9].

The corrosion of dual phase steels has not yet been explored extensively, and only a few studies have been reported [2,10] showing that the low corrosion resistance of dual phase steel is greatly influenced by the microstructure and test conditions. Galv-annealed (GA) coating for dual-phase steels have been used with the intention of improving corrosion resistance. However, few microstructure studies of GA coatings have been conducted because of the difficulty of sample preparation [9]. In this study pack boronizing treatment was preferred as it is easy to apply, cheaper and has superior properties. Boronizing is a thermo-chemical diffusion process in which boron is diffused to steel under a high temperature [11]. It has excellent properties such as high hardness (1400–3000 HV), very low friction coefficient [11], resistance to corrosion (acid and base medium) [12,13] and high temperature oxidations [14].

In this study the electrochemical corrosion behaviors in a 3.5 wt.% NaCl solution with respect to the variation in the number and morphology of the phase constituents developed through batch intercritical annealing of boronized dual-phase (BDP) steel were examined. The corrosion data were obtained through the Tafel extrapolation and lineal polarization electrochemical techniques. The corrosion resistance of boronized samples was comparable to that of dual-phase steels.

2. Experimental details

2.1. Material and heat treatment

AISI 1010 dual-phase steel, whose chemical composition is given in Table 1, was used in the electrochemical corrosion experiments. Cylindrical specimens with a diameter of 15 mm and length of 10 mm were used in the corrosion tests. Specimens were coded as DP32, DP61, DP81, BDP32, BDP61 and BDP81. Coding and descriptions are shown in Fig. 1.

Samples are subjected to different heat treatment regimes as follows:

(i) Intercritical annealing of the specimens at 760 °C, 790 °C and 820 °C for 30 min and finally, quenching (DP32, DP61 and DP81).

* Corresponding author. Tel.: +90 272 228 13 11; fax: +90 272 228 13 19.
E-mail address: ykayali@aku.edu.tr (Y. Kayali).

0261-3069/$ - see front matter
http://dx.doi.org/10.1016/j.matdes.2012.11.040

Table 1
Chemical composition of test materials (wt.%).

Element	C	Mn	Si	Ni	Cr	Al	Co	S
wt.%	0.151	0.730	0.175	0.105	0.067	0.047	0.010	0.017

(ii) Boronizing was performed in a solid medium containing commercial Ekabor-2 powder under atmospheric pressure at a temperature of 900 °C for 2 h. This was followed by intercritical annealing of the martensitic structure at 720 °C, 760 °C and 780 °C for 30 min and finally, quenching (BDP32, BDP61 and BDP81).

The summary of the heat treatments is shown in Fig. 1.

Boronizing was performed in a solid medium using Ekabor-2 powders which had a nominal chemical composition of 90% SiC, 5% B_4C and 5%KBF_4. Boronizing treatment was performed at 900 °C for 2 h. All the heat treatment regimes were carried out in a tube furnace under air atmosphere. After the intercritical temperatures the specimens were cooled in oil to room temperature with adequate stirring for a uniform heat transfer.

Microstructure of the specimens was observed under a light microscope following the usual metallographic polishing and etching with 2% nital solution. Volume fraction of the phase constituents was determined by using an automatic image analyzer (MicroCAM 4.1). The hardness of the boride layers and substrates was measured at the cross-sections using a Shimadzu HMV-2 Vickers indenter with a 50 g load.

The microstructures of polished and etched cross-sections of the samples were observed by an optical microscope (Olympus BX-60) and scanning electron microscopy-energy dispersive X-ray spectrometer (SEM-EDS) (Leo 1430VP). The presence of borides formed in the coating layer was confirmed by means of X-ray diffraction (Shimadzu XRD-6000) using Cu Kα (λ = 1.5406 Å) radiation. The measurement of the layer thickness has some difficulties because of saw tooth morphology of boride layer. Therefore, different descriptions have made. In literature, layer thickness of boride layer have been calculated by taking average distance of every columnar from the surface [15,16]. The thickness of the boride layer on the dual-phase steel was measured by means of a digital thickness measuring instrument attached to an optical microscope. The measured thickness values were given as averages of at least 10 measurements.

2.2. Corrosion test

Samples were grounded from rough emery grit paper to fine emery grit paper and were washed in bidistilled water by ultrasonic bath. They were subsequently washed with acetone, alcohol, and bidistilled water in a Bandelin ultrasonic bath for 15 min at 30 °C. Then, substrates were dried at 40 °C for one hour in a drying oven. Solutions were prepared in bidistilled water using Merck grade reagents. Measurements were obtained using a system consisting of a Reference 600 potentiostat/galvanostat/ZRA (Zero Resistance Ammeter) system supported by the Echem Analyst Soft Programme. Corrosion experiments were carried out after the samples were left waiting for 1 h at room temperature (25 °C) in a 3.5 wt.% NaCl solution (pH 6.8). A conventional three-electrode cell was used for all the electrochemical measurements. A saturated calomel electrode (SCE) was used as a reference electrode, platinum foil as a counter electrode and AISI 1010 dual-phase steel substrates as the working electrode. All potentials were referred to the saturated calomel electrode. In order to test the reproducibility of the results, the experiments were always repeated at least five times. To determine the corrosion rates, the anodic and cathodic Tafel regions extrapolating to corrosion potentials were used. The polarization resistance values were calculated from linear zones of current–potential curves near the corrosion potential.

3. Results and discussion

3.1. Microstructure

Fig. 2 shows the optical and SEM micrographs of non-treatment specimens (Ferrite + pearlite = FP). It shows that the as-received specimens consist largely of the ferrite matrix phase (light area) and pearlite (dark area) at the grain boundaries. Microstructures of DP steels developed using intercritical temperatures are shown in Fig. 3.

If we examine Fig. 3a, it can be seen that there is a development of a martensite network surrounding the polyhedral ferrite grains. The volume fraction of the developing network of martensite is 32%. Such a morphological distribution of martensite is commonly known as a chain or a continuous network of martensite. It is thus revealed that formation of austenite during the intercritical annealing structure favorably occurs through nucleation of austenite at ferrite–ferrite boundaries [2,17]. The microstructure shown in Fig. 3b, as representative of DP61 specimens, reveals a uniform distribution of island martensite in a ferrite matrix. The DP81 structure shown in Fig. 3c consists of 81% of the volume fraction of martensite. The DP81 specimen reveals a uniform distribution of island ferrite in a martensite matrix. Fig. 3 shows that the amount of martensite increases with an increase in the intercritical annealing temperature. The reason why the amount of martensite increases with the temperature is that more austenite is present at

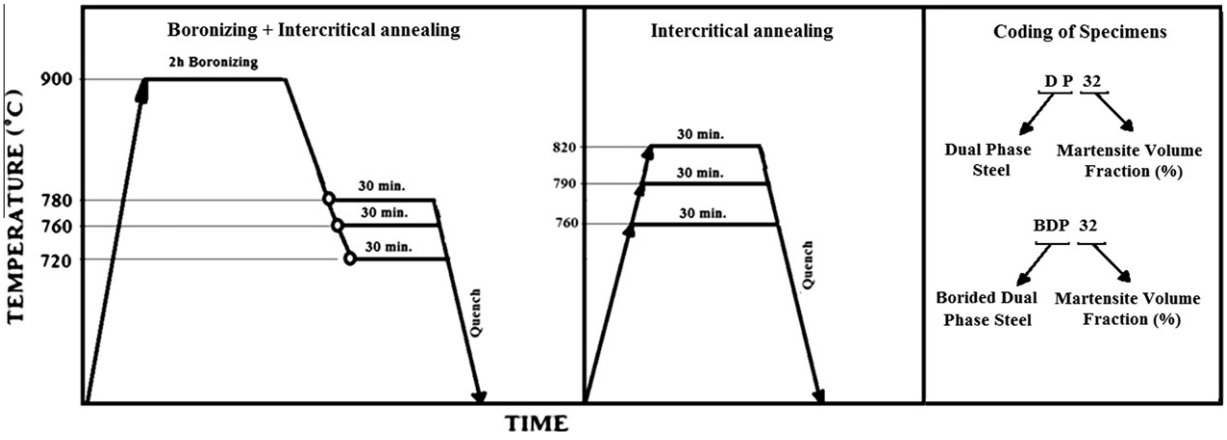

Fig. 1. Summary of heat treatments and coding descriptions.

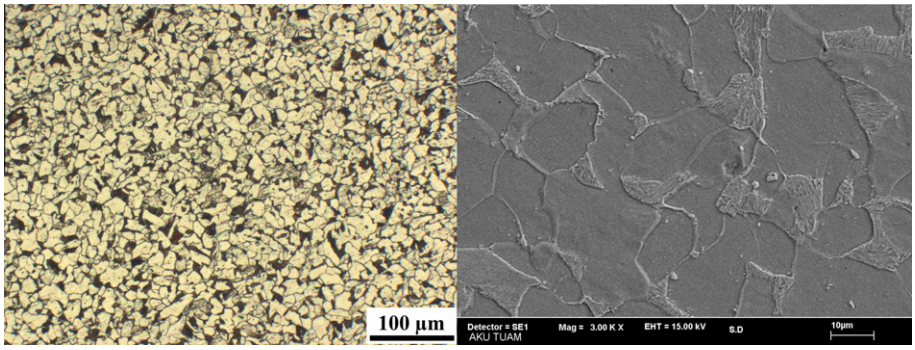

Fig. 2. Microstructure of non-treatment ferrite/pearlite structure (FP specimen).

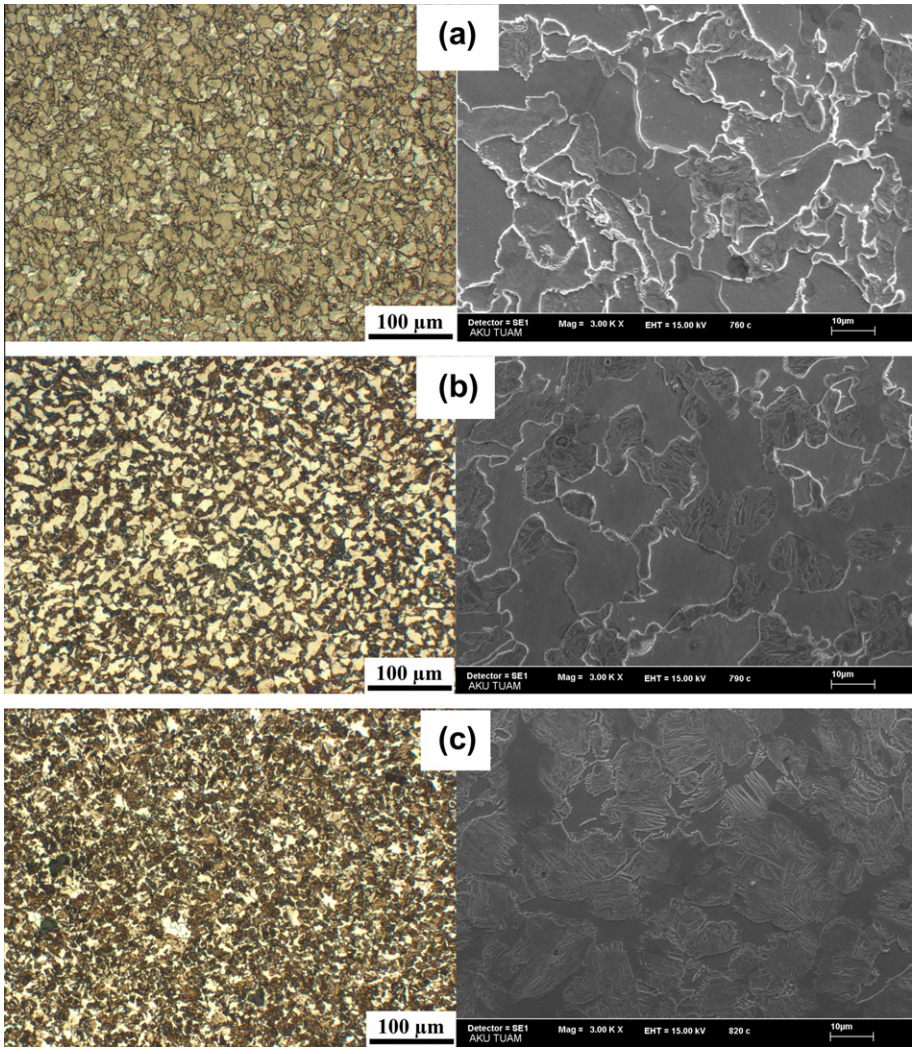

Fig. 3. Microstructure of dual-phase steels: (a) DP 32, (b) DP 61 and (c) DP 81.

higher temperatures. Thus, martensite is present to a higher extent after quenching [2,6]. The microstructure photos of boronized dual-phase steels are presented in Fig. 4. As a result of metallographical investigation of boronized dual-phase steels it was determined that the boride layer had a toothed structure and this structure was homogeneously distributed over the surface [18]. The coating layer occurring on boronized-dual-phase steel consists of 3 zones. Zone 1; Boride layer (FeB and Fe_2B), Zone 2 is a transition zone. The zone consists of a solid solution of boron and has a lower hardness than the boride layer. Zone 3 is a matrix [18–20].

Martensite volume fraction in the structure of the matrix of the boronized dual-phase steels increased (from 32% to 81%) with the increase in the intercritical temperature (from 720 °C to 780 °C).

The X-ray diffraction patterns of boronized-dual-phase steel at different intercritical annealing temperatures are given in Fig. 5. XRD results showed that the boride layers formed on the DP steels contained FeB and Fe_2B. The properties of these boride layers are known to a large extent by the help of these phases [21,22]. While the FeB phase formed near the surface, the Fe_2B phases formed between FeB and the matrix interface [23]. The FeB phase decreases

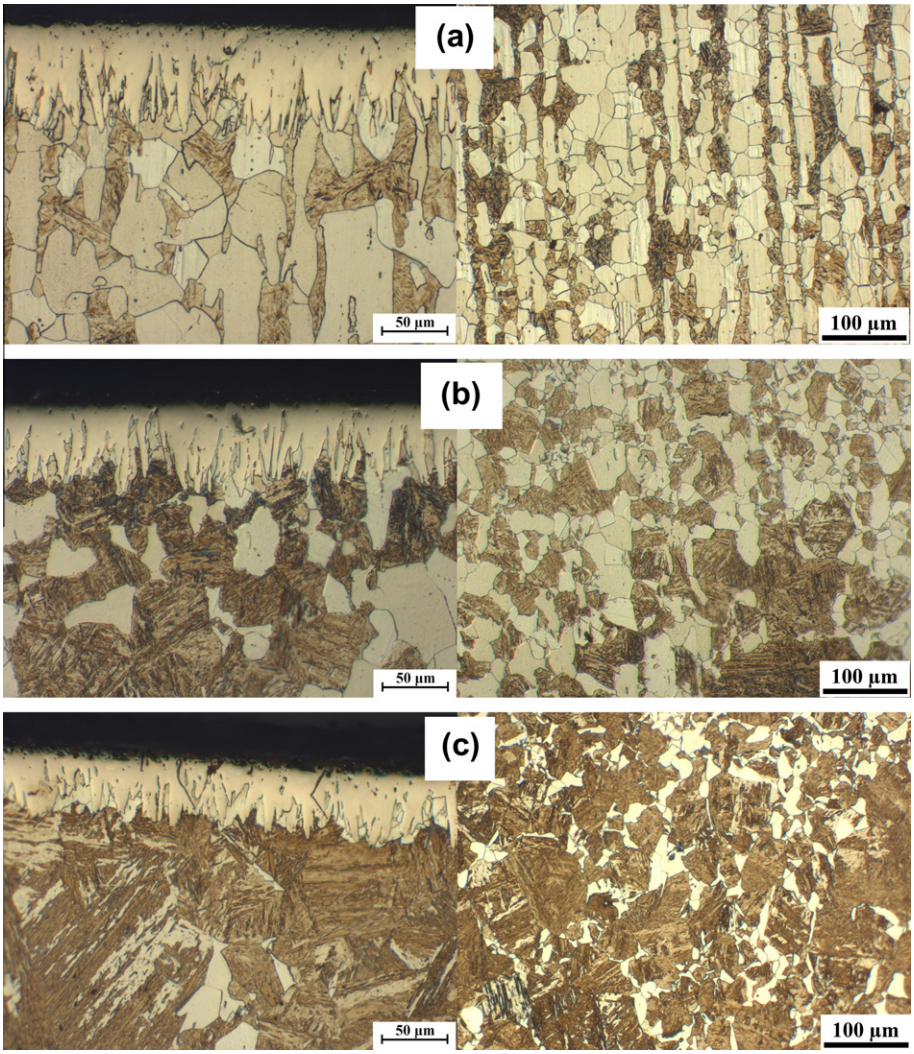

Fig. 4. Microstructure of Boronized dual-phase steels: (a) BDP 32, (b) BDP 61 and (c) BDP 81.

while the Fe_2B phase increases with the increase in the intercritical temperature. Thus, the Fe_2B phase becomes dominant on the surface of the boride layer.

The boride layer thicknesses on the dual phase steels obtained at different intercritical annealing temperatures are between 50 and 70 µm. Hardness values were carried out by using a Vickers type. Microhardness measurements were calculated based on the average of at least 10 measurements carried out on the boride layer (Table 2). The maximum hardness of the boride layer was determined to be 1643 $HV_{0.05}$. As a result of the increase in the rate of martensite, matrix hardness rose from 206 $HV_{0.05}$ to 450 $HV_{0.05}$. The matrix hardness increased approximately 4–5 folds with the boronizing process [20]. With the increase in the intercritical temperature, the Fe_2B phase became more dominant and thus the hardness of the boride layer decreased [11,24].

3.2. Corrosion behavior

The results of the corrosion experiments of the developed materials according to a standard calomel electrode are shown in Table 3. The data for the corrosion potential (E_{corr}), corrosion current density (i_{corr}), corrosion resistance (Rp) and corrosion rate shown in Table 3 have been derived from the experimentally obtained cathodic and anodic polarization (E vs. $\log I$) curves using Tafel extrapolation and linear polarization methods.

In the present study mainly three types of materials were selected: The first material had a ferrite-pearlite microstructure. The second one was a dual phase steel with a different ferrite–martensite microstructure obtained at different intercritical heat treatment temperatures. The third one was a boron-coated dual-phase steel with a different ferrite-martensite microstructure obtained at different intercritical heat treatment temperatures. It was observed that depending upon microstructure, i.e., phase constituents, phase composition and morphologies, the corrosion rate of the dual-phase steel under study varied in a 3.5 wt.% NaCl environment.

Tafel curves of boronized and non-boronized dual-phase steels in a 3.5 wt.% NaCl solution are given in Fig. 6a and b. Fig. 6 and Table 3 show that the corrosion current density (i_{corr}), is lower for FP steel as compared to both the BDP and DP samples. With the change in microstructure from ferrite-pearlite to ferrite-martensite the corrosion current density and the corrosion rate increase and hence corrosion resistance decreases. While the i_{corr} varied between 6.738 and 17.677 µA cm^{-2} in non-boronized dual-phase steels, the corrosion current density in the boronized samples varied between 3.664 and 5.946 µA cm^{-2}. The corrosion rates of the non-boronized samples increased compared to the boronized ones.

Among the different DP steels the i_{corr} values were found to depend on the relative number of phase constituents. The i_{corr} value

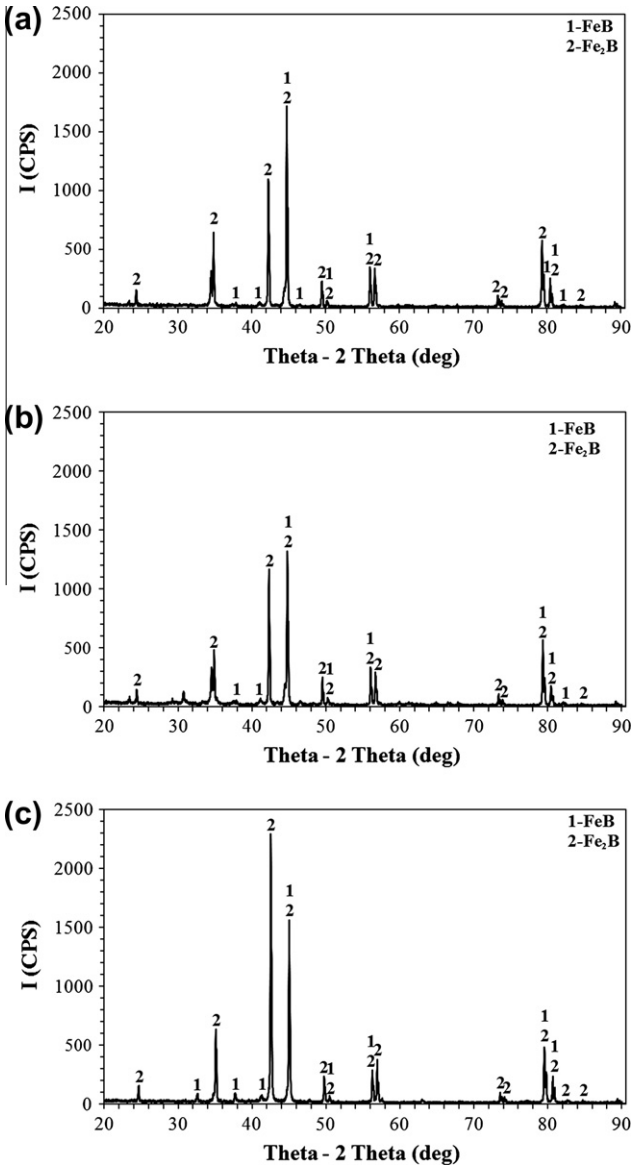

Fig. 5. X-ray diffraction patterns observed from the surface of the boronized dual-phase steels: (a) BDP 32, (b) BDP 61 and (c) BDP 81.

was found to increase with the amount of martensite [2,10]. Despite the fact that the martensite morphologies of the BDP32 and DP32, BDP61 and DP61, BDP81 and DP81 remain almost the same, the $i_{corr.}$ values of the borided steels decrease. This shows us that corrosion resistance increases with boriding process. The corrosion resistance of borided dual-phase steel is weaker than that of FP steel. The reason behind this may be related to the porosities and pores on the boron layer. The corrosion resistance of boron-coated steel usually depends on the characteristic features of coatings such as the number of microcracks and porosities. These porosities negatively affect the firmness of coatings and significantly reduce the corrosion resistance. The number of these voids is associated with the microstructure of the coating [25,26].

In the corrosion of the samples in a neutral 3.5 wt.% NaCl solution, the following corrosion reactions take place at the same time [10].

$$\text{Anodic reaction}: Fe \rightarrow Fe^{2+} + 2e^{-} \quad (1)$$

$$\text{Cathodic reaction}: O_2 + 2H_2O + 4e^{-} \rightarrow 4OH^{-} \quad (2)$$

As seen in Table 3, following as a result of the increase in the amount of martensite brought about by employing a higher intercritical temperature, the amount of ferrite decreases. Such a change in the number of the phase constituents leads to a change in the ratio of cathode to anode areas. Thus, with the rise of the intercritical temperature from 760 °C to 820 °C and with the increase in the amount of martensite, the highest corrosion rate was observed in DP81 steel. This study shows an increased corrosion rate for the DP81 material compared to the BDP61, DP61 specimens, respectively. This occurs due to the variation in the morphology and distribution of the phase constituents [17].

While the increase in the intercritical temperature leads to a reduction in the amount of ferrite (anode) and an increase in the amount of martensite (cathode), therefore, the $i_{corr.}$ value and corrosion rate increase. The corrosion rate of DP steel is influenced by both the volume fraction and the morphology of the constituting phases in such a manner that an increased amount of martensite leads to an increase in the corrosion rate of DP steel.

The corrosion resistance of the boronized dual phase steel is higher, the i_{corr} value is lower and therefore the corrosion rate is lower compared to the dual-phase steels with the same matrix structure (BDP32-DP32, BDP61-DP61, and BDP81-DP81). As is clear from these results, the boriding process increases the corrosion resistance of dual phase steels.

SEM-EDS images of samples after electrochemical tests in a 3.5 wt.% NaCl solution following immersion times of 1 h are given in Fig. 7 and Table 4.

It is observed that Na^+, Cl^-, O^{2-} ions from the solution are present in the EDS analysis. When Table 4 is analyzed, it appears in the EDS analysis that there are very few Na^+ and Cl^- elements on the surface of the FP samples which have the best corrosion resistance. It was determined that an oxide layer was formed on the surface of the boronized samples during the corrosion tests (Fig. 7a). This oxide layer indicates that it reduces the anodic dissolution and that the boride layer provides more effective protection. The oxide layer formed due to the decrease in the corrosion rate of the samples is

Table 2
Summary of result obtained from hardness.

Specimen code	Microstructure	Volume of martensite	Hardness of boride layer ($HV_{0.05}$)	Hardness of matrix ($HV_{0.05}$)	
				Ferrite	Perliate
FP	Ferrite–pearlite	–	–	170	224
				Ferrite	Martensite
DP 32	Ferrite-chain martensite	32	–	254	331
DP 61	Island martensite in continuous ferrite matrix	61	–	263	371
DP 81	Island ferrite in continuous martensite matrix	81	–	283	395
BDP 32	Ferrite-chain martensite	32	1643	246	431
BDP 61	Island martensite in continuous ferrite matrix	61	1512	258	435
BDP 81	Island ferrite in continuous martensite matrix	81	1325	292	450

Table 3
Summary of result obtained from corrosion tests performed in 3.5 wt.% NaCl solution.

Specimen code	Microstructure	Volume of martensite	Corrosion current density, $i_{corr.}$ (μA/cm^2)	Corrosion potential $E_{corr.}$ (mV)	Corrosion rate ($\times 10^{-3}$) (mpy)	Corrosion resistance Rp (kΩ)
FP	Ferrite–pearlite	–	2424	−701	1090	5002
BDP 32	Ferrite-chain martensite	32	3664	−739	1649	2189
BDP 61	Island martensite in continuous ferrite matrix	61	5045	−774	2272	2098
BDP 81	Island ferrite in continuous martensite matrix	81	5946	−766	2669	2060
DP 32	Ferrite-chain martensite	32	6738	−717	3027	1124
DP 61	Island martensite in continuous ferrite matrix	61	12,118	−723	5495	0570
DP 81	Island ferrite in continuous martensite matrix	81	17,667	−736	7940	0284

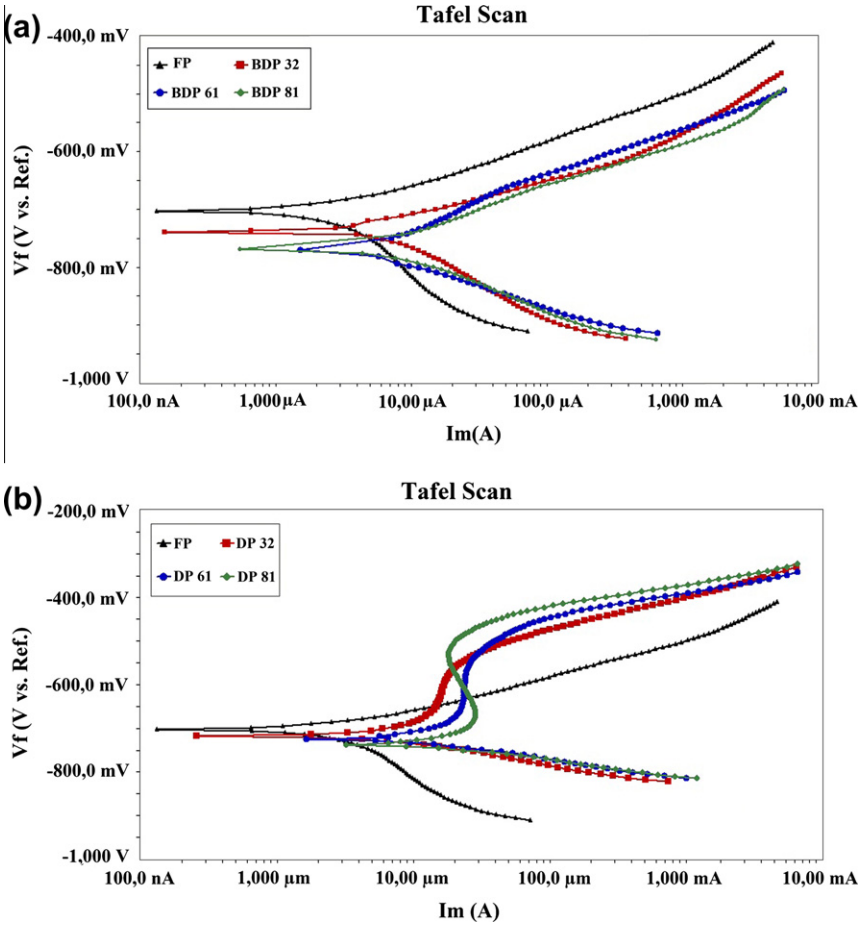

Fig. 6. Tafel curves of (a) boronized and (b) non-boronized dual-phase steels.

thought to have a protective effect [27,28]. Amount of Cl^- and iron ions are quite high on the surface of the dual-phase steels after corrosion tests as shown in the Table 4 and Fig. 7b. However, ratios of iron and oxygen ions on the surface of dual-phase steels after corrosion tests decreased. And Na^+ and Cl^- ions are adsorbed from solution to the surface of samples. This adsorbed aggressive Cl^- ions formed a soluble complex salts with iron ions on the surface. It can be considered that this soluble complex salts caused the pitting corrosion on the dual-phase steels. It was determined that the amounts of Na^+ and Cl^- on the surface of the dual-phase samples with poor corrosion resistance increased while the amount of O^{2-} on the surface of the boronized samples decreased (Fig. 7).

4. Conclusions

In this study, corrosion behaviors of boronized and non-boronized dual-phase steel were investigated in a 3.5 wt.% NaCl solution. The following conclusions can be drawn from the results:

(1) As a result of metallographic examinations of the boronized samples, it was observed that the coating-matrix interface morphology has a flat and saw smooth morphology.
(2) It was determined through X-ray diffraction analysis that the FeB and Fe_2B phases are present on the material surface as a result of boronizing.

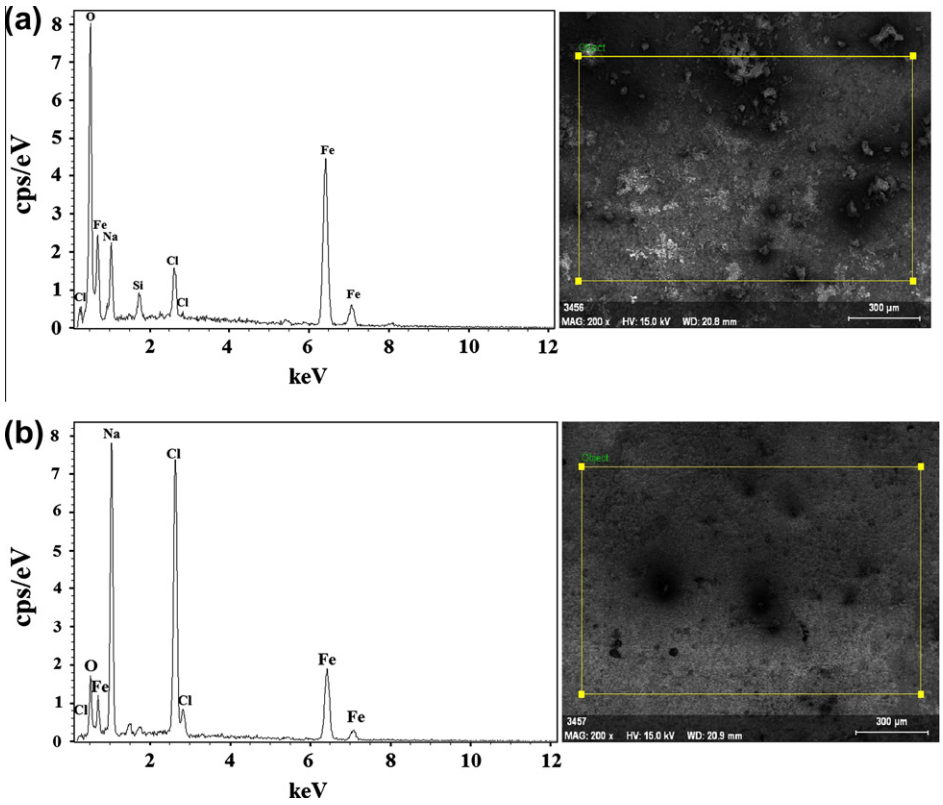

Fig. 7. EDS analyses of dual-phase steel surface in 3.5% NaCl solution (a) BDP 32 and (b) DP 81.

Table 4
EDS quantative element analyses (% atom).

Specimen code	Elements					
	O	Na	Cl	S	Si	Fe
FP	–	1.54	0.5	–	–	97.93
BDP 32	32.56	9.73	3.25	–	1.42	53.09
BDP 61	30.25	9.24	2.11	1.58	–	56.82
BDP 81	24.22	9.33	5.26	–	–	61.69
DP 32	22.21	10.21	5.89	–	–	61.19
DP 61	14.39	19.46	13.97	–	0.93	42.38
DP 81	8.52	29.44	24.64	–	–	37.39

(3) The martensite ratio in dual-phase steel and borided dual-phase steel increased with an increase in the intercritical annealing temperature. The corrosion resistance decreased with increase of the martensite ratio.
(4) The boride layer increased the corrosion resistance of dual phase steel 2–3-fold.
(5) The superior properties of the dual phase steel as well as poor corrosion properties were improved by the boriding process.

Acknowledgements

The authors are grateful to the Scientific Research Project Council of Afyon Kocatepe University (Project Number: 11.FEN.BİL.32). This article was written based on B. Anaturk's master thesis.

References

[1] Abouei V, Saghafian H, Kheirandish Sh, Ranjbar Kh. An investigation of the wear behaviour of 0.2% C dual phase steels. J Mater Process Technol 2008;203:107–12.
[2] Sarkar PP, Kumar P, Manna MK, Chakraborti PC. Microstructure influence on the electrochemical corrosion behaviour of dual-phase steels in 3.5% NaCl solutions. Mater Lett 2005;59:2488–91.
[3] Erdogan M, Priestner R. Effect of epitaxial ferrite on yielding and plastic flow in dual phase steel in tension and compression. Mater Sci Technol 1999;15:1273–84.
[4] Sarwar M, Ahmad E, Qureshi KA, Manzoor T. Influence of epitaxial ferrite on tensile properties of dual phase steel. Mater Des 2007;28:335–40.
[5] Erdogan M. Effect of austenite dispersion on phase transformation in dual phase steel. Scripta Mater 2003;48:501–6.
[6] Maleque MA, Poon YM, Masjuki HH. The effect of intercritical heat treatment on the mechanical properties of AISI 3115 steel. J Mater Process Technol 2004;153–154:482–7.
[7] Gündüz S. Effect of chemical composition, martensite volume fraction and tempering on tensile behaviour of dual phase steels. Mater Lett 2009;63:2381–3.
[8] Bayram A, Uguz A, Ula M. Effect of microstructure and notches on the mechanical properties of dual-phase steels. Mater Charact 1999;43:259–69.
[9] Kao FH, Li WC, Chen CY, Huang CY, Yang JR, Wang SH. Cross-sectional observation of the intermetallic phase in a galvannealed steel. Mater Sci Eng, A 2009;499:45–8.
[10] Bhagavathi LR, Chaudhari GP, Nath SK. Mechanical and corrosion behavior of plain low carbon dual-phase steels. Mater Des 2011;32:433–40.
[11] Sinha AK. Boriding (boronising). ASM handbook J Heat Treatment 1991;4:437–47.
[12] Ozbek I, Sen S, Ipek M, Bindal C, Zeytin S, Üçışık AH. A mechanical aspect of borides formed on the AISI 440C stainless-steel. Vacuum 2004;73C:643–8.
[13] Pertek A, Kulka M. Microstructure and properties of composite (B + C) diffusion layers on low-carbon steel. J Mater Sci 2003;38:269–73.
[14] Yan PX, Zhang XM, Xu JW, Wu ZG, Song QM. High-temperature behavior of the boride layer of 45# carbon steel. Mater Chem Phys 2001;71:107–10.
[15] Matushcka AG. Boronising. Carl Hanser Verlag: Munchen Wien; 1987. 100.
[16] Campos I, Torres R, Ramirez G, Ganem R, Martinez J. Growth kinetics of iron boride layers: dimensional analysis. Appl Surf Sci 2006;252:8662–7.
[17] Navara E, Bengtsson B, Easterling KE. Austenite formation in manganese-partitioning dual-phase steel. Mater Sci Technol 1986;12–2:1196–201.
[18] Atik E, Yunker U, Meric C. The effects of conventional heat treatment and boronizing on abrasive wear and corrosion of SAE 1010, SAE 1040, D2 and 304 steels. Tribol Int 2003;36:155–61.
[19] Sen S. The characterization of vanadium boride coatings on AISI 8620 steel. Surf Coat Technol 2005;190:1–6.
[20] Genel K, Ozbek I, Bindal C. Kinetics of boriding of AISI W1 steel. Mater Sci Eng, A 2003;347:311–4.

[21] Kayali Y, Günes I, Ulu S. Diffusion kinetics of borided AISI 52100 and AISI 440C steels. Vacuum 2012;86:1428–34.
[22] Uslu I, Comert H, Ipek M, Celebi FG, Ozdemir O, Bindal C. A comporasion of borides formed on AISI 1040 and AISI P20 steels. Mater Des 2007;28: 1819–26.
[23] Uslu I, Comert H, Ipek M, Ozdemir O, Bindal C. Evaluation of borides formed on AISI P20 steel. Mater Des 2007;28:55–61.
[24] Kartal G, Kahvecioglu O, Timur S. Investigating the morphology and corrosion behavior of electrochemically borided steel. Surf Coat Technol 2006;200:3590–3.
[25] Liu C, Lin G, Yang D, Qi M. In vitro corrosion behavior of multilayered Ti/TiN coating on biomedical AISI 316L stainless steel. Surf Coat Technol 2006;200:4011–6.
[26] Campos I, Palomar M, Amador A, Ganem R, Martinez J. Evaluation of the corrosion resistance of iron boride coatings obtained by paste boriding process. Surf Coat Technol 2006;201:2438–42.
[27] Uneri S. Corrosion and its prevention. Ankara: Corrosion Society Publications; 2000.
[28] Schweitzer PA. Fundamentals of metallic corrosion: atmospheric and media corrosion of metals. 2nd ed. New York: CRC Press; 2007.